Scientific Visualization, 2023, volume 15, number 4, pages 41 - 55, DOI: 10.26583/sv.15.4.04

Application of Scientific Visualization in Low-Temperature Gas Discharge Plasma Modeling

V.P. Budak[1], I.I. Zheleznov[2]

National Research University "Moscow Power Engineering Institute"

[1] ORCID: 0000-0003-4750-0160, budakvp@gmail.com
[2] ORCID: 0009-0004-8875-2991, zheleznov96y@gmail.com

Abstract

This article discusses the importance of developing software and hardware complexes for data visualization and improving methods of presenting them in the modeling of low-temperature gas discharge plasma phenomena and related physical processes. In particular, issues related to creating a specialized distributed environment for solving gas discharge modeling tasks are considered. The use of computer graphics for visualization has allowed for a visual analysis of the obtained data and making necessary adjustments to the modeling process interactively with the data. The paper presents the results of visualizing a model of mercury-argon plasma in a coaxial microwave discharge. The application of local cross-sections of the computational domain for visualization has revealed the internal structure and peculiarities of the distribution of the electric field and electron concentration in the discharge tube. The obtained data served as the basis for creating an experimental prototype of a coaxial gas discharge optical radiation source.

Keywords: Data Visualization, Low-Temperature Plasma Modeling, Gas Discharge Plasma.

1. Introduction

Visualization technologies are most commonly applied in tasks involving numerical modeling of complex, multi-component models when teraflop-level computational resources are required. Due to the high complexity of the objects under investigation, constructing computational grids can pose significant challenges. Determining the optimal sizes and structures of computational grids required to achieve acceptable accuracy implies the need to adjust model parameters. This process becomes iterative and interactive, as visualization results help analyze and adjust grid parameters. To achieve desired results when analyzing raw data using scientific visualization, the calculation and visualization algorithm must be repeatedly executed, with changes made to various parameters and real-time visual assessment of intermediate results.

A special role in visualizing modeling results is played in low-temperature plasma research. In recent years, there has been a rapid increase in work related to self-consistent modeling of complex gas discharge plasma systems, especially [1-3]. This is due to two reasons. Firstly, it involves accumulating reliable databases of various constants used in modeling (cross-sections of various processes, transport coefficients, reactions, etc.). Secondly, it involves an increase in the computing power used for calculations, allowing for more complex problem-solving closer to experimental descriptions and obtaining results in a short time. Furthermore, while one-dimensional and two-dimensional problems were previously solved, the development of three-dimensional models has become relevant with the advent of powerful computing resources.

The process of visualizing data in low-temperature gas discharge plasma radiation modeling is a task that involves considering the unique characteristics of this state of matter

and requires careful adjustment of the visual representation of the obtained results. Unlike similar tasks associated with higher-temperature plasma states, such as plasma in the solar corona or tokamak-type devices, where thermal motion of particles plays a more significant role, low-temperature gas discharge plasma exhibits more pronounced chemical activity and interaction with neutral atoms and molecules.

Therefore, successful data visualization of this process requires the use of specialized methods capable of taking into account the unique characteristics of low-temperature plasma and conveying information about molecular and chemical interactions, which play a significant role in this context:

1. *Colorimetry and contour diagrams*: This approach relies on the use of various colors and color scales to demonstrate plasma parameters. This allows for the visualization of, for example, radiation intensity or particle density. The use of contour diagrams helps highlight lines representing constant parameter values, facilitating the detection of structures and patterns.
2. *Isolines and isosurfaces*: In this method, isolines are used, which are curves connecting points with the same parameter values. Isosurfaces, in turn, represent shaded areas between isolines, colored depending on the parameter level. This method allows for the detection of gradients and changes in plasma parameters.
3. *Volume visualization (3D visualization)*: To gain a deeper understanding of plasma structure, volume visualization is used. It provides the opportunity to observe structures in three-dimensional space and interact with them.
4. *Animation and temporal visualization*: In cases where plasma modeling involves temporal dynamics, animations become informative. This approach allows for tracking changes in plasma parameters over time and identifying dynamic processes.

However, when using the above-mentioned methods, researchers face several difficulties and limitations:

- Modeling complexity: Gas discharge plasma is a complex system with many interacting particles, energy processes, and chemical reactions. Modeling such plasma requires taking into account all these factors, which is a computationally intensive task. The need to consider numerous transitions and interactions between plasma components complicates modeling and requires significant computational resources.
- Database limitations: Modeling radiation requires databases of emission spectra for various elements and molecules in plasma. However, some data may be incomplete or unavailable for certain elements or plasma conditions, reducing modeling accuracy.
- Three-dimensional geometry consideration: Low-temperature plasma often has complex three-dimensional geometry, such as discharge chambers or electrodes. Accounting for such geometry in modeling and visualization can be a challenging task and requires the use of appropriate 3D computer graphics algorithms.
- Computational resource constraints: Modeling and visualizing radiation processes in gas discharge plasma require significant computing power. Calculations can be time-consuming, especially when using high-resolution 3D models and complex ray tracing algorithms. Limited resources can affect modeling accuracy and result retrieval time.
- Model validation: Ensuring model accuracy requires validation. This can be a challenging task since experimental data may be limited or unavailable. It is essential to perform model adequacy checks and compare results with available experimental data.

Considering all these aspects, the specificity of data visualization in modeling low-temperature gas discharge plasma radiation requires the development of specialized methods and tools capable of accounting for the unique characteristics of this type of plasma. These methods and tools provide researchers with the ability to conduct a comprehensive analysis and interaction with computational results. Given the ongoing development of computer technologies and the refinement of physical models, the mentioned difficulties can be overcome, ultimately allowing for more accurate and realistic visualizations of plasma processes [4, 5].

2. Model Parameters

As the subject of study, let's consider an example of visualizing a coaxial mercury-argon discharge excited by the microwave electromagnetic field of a magnetron [6].

Given that, under the studied conditions and the geometry of the discharge system, the electron energy relaxation length significantly exceeds the radius of the discharge tube, a self-consistent model is used to describe the discharge in the approximation of local thermodynamic equilibrium (LTE). This condition is applicable in the region of mercury pressures on the order of 0.05 Torr, argon pressures around 0.1–0.7 Torr, and a discharge tube radius of 1–3 cm.

Thus, in the case of cylindrical geometry of the discharge tube, the boundary conditions for the equation of balance between the formation and destruction of charged particles can be expressed as follows [7]:

$$\nabla n_e\big|_{r=0} = 0,\ -D_a \nabla n_e\big|_{r=R} = n_e(R) V_i = n_e(R)\sqrt{\frac{kT_e}{M_i}} \tag{1}$$

Here, R is the radius of the tube, k is the Boltzmann constant, and D_a is the coefficient of ambipolar diffusion. $V_i = \sqrt{kT_e / M_i}$ – the ion sound velocity, M_i is the velocity of an ion that has passed through an accelerating potential difference $0.5kT_e / e$, e — elementary charge.

In this case, there is no local connection of the parameters of the electronic component with the microwave field, and it is replaced by the balance equation for the electron energy flux density.

The concentration of electrons in the discharge will be approximated using the zero-order Bessel function:

$$n_e(r) = n_{e0} J_0(\alpha r/R),\ r = \sqrt{x^2 + y^2}\,, \tag{2}$$

where α – a coefficient that takes into account the difference in the electron concentration near the walls from zero, determined from the boundary condition:

$$-\frac{\mu_i kT_e}{e}\frac{\partial}{\partial r} J_0(\alpha r/R)\bigg|_{r=R} = J_0(\alpha)\sqrt{\frac{kT_e}{M_i}}\,, \tag{3}$$

where μ_i and M_i – mobility and mass of mercury ion.

The mobility of mercury ions in mercury and argon is not difficult to determine, according to [8]:

$$\mu_i^{Hg} = 0.24\times10^{-4}\left[\frac{1.0132\times10^5 T}{500\, p_{Hg}}\right], \tag{4}$$

$$\mu_i^{Ar} = 1.84\times10^{-4}\left[\frac{1.0132\times10^5 T}{300\, p_{Hg}}\right]. \tag{5}$$

Here p_{Hg} & p_{Ar} – pressure in Torr, T - gas temperature in Kelvin. Then the final mobility of mercury ions in a mixture of mercury and argon will be determined as:

$$\mu_i = \left(\frac{1}{\mu_i^{Hg}} + \frac{1}{\mu_i^{Ar}}\right)^{-1}, \tag{6}$$

Assume that the distribution of the electron concentration along the radius is stationary. It is easy to prove this by comparing the relaxation time of the electron concentration τ_a, due to ambipolar diffusion, with the oscillation period of the supply voltage. In this case, the condition must be met:

$$\frac{1}{2\pi f \tau_a} \ll 1 \tag{7}$$

where f – frequency of supply voltage fluctuations, and τ_a can be calculated [9] using the following relation:

$$\tau_a = R^2 (2.405^2 D_a)^{-1}. \quad (8)$$

In this case, the criterion of stationarity:

$$\gamma = \frac{2.405^2 D_a}{2\pi f R^2} \ll 1 \quad (9)$$

.

Let's determine the diffusion coefficient of mercury atoms D. So, for a mercury-argon mixture [10]:

$$D = 1.858 \times 10^{-7} T^{3/2} \frac{\sqrt{(M_{Hg} + M_{Ar}) / M_{Hg} M_{Ar}}}{\sigma^2 \Omega \cdot \left(p_{Hg} + p_{Ar} \right) / 101325}, \frac{m^2}{s}. \quad (10)$$

where $M_{Hg} = 200.59$; $M_{Ar} = 39.948$; $\sigma = 3.2555$ Å – characteristic interaction distance of mercury and argon, Ω – collision integral for diffusion.

In turn, the mobility of electrons can be determined using the concept of the electron energy distribution function:

$$\mu_e = -\frac{2e}{3m_e} \int_0^\infty \frac{U^{3/2}}{\nu_m + j\omega} \frac{\partial}{\partial U} \left[\frac{f(U)}{\sqrt{U}} \right] dU, \quad (11)$$

where $\nu_m = \nu n_{Hg} Q_{m,Hg}(\nu) + \nu n_{Ar} Q_{m,Ar}(\nu)$ – transport frequency of elastic electron scattering on mercury and argon atoms, $f(U)$ – the unit-normalized electron energy distribution function (EEDF):

$$\int_0^\infty f_e(U) dU = 1. \quad (12)$$

The relative permittivity of the dispersion medium was calculated using the Drude model [11]. In this model, the collision frequency ν_m, the plasma electron frequency ω_{pe} and the breakdown field E_c are the three key parameters. The plasma frequency of the electron ω_{pe} was determined using the equation:

$$\omega_{pe} = \sqrt{\frac{n_e e^2}{\varepsilon_0 m_e}}, \quad (13)$$

here m_e — electron mass.

At the same time, the frequency of collisions of ν_m electrons with neutral atoms:

$$\nu_m = \frac{\sqrt{8kT_e / \pi m_e}}{\lambda_e}, \quad (14)$$

where T_e — electron temperature, λ_e — the free path length between neutral atoms and electrons.

The electric field strength of the breakdown E_c was expressed by the equation:

$$E_C = \frac{kT\omega}{psA\sqrt{\frac{m_e \nu_i}{3e}}}, \quad (15)$$

where υ_i is the ionization potential of a neutral particle, ω is the circular frequency of microwaves), s is the elastic collision cross—section, T is the temperature of the working mercury–argon mixture, Λ is the characteristic length of electron diffusion in the cylinder:

$$\Lambda = \frac{1}{\sqrt{\left(\frac{\pi}{l} \right)^2 + \left(\frac{2,405}{R} \right)^2}}, \quad (16)$$

where l is the length of the tube, R is the inner diameter of the cylinder.

Now it is necessary to evaluate the interaction of radiation with plasma components. To do this, imagine the radiation transfer in a two-level system. Let n_1, n_2 be the concentrations of atoms at levels 1 and 2. We formulate the kinetic equation for the concentration of particles at the second level:

$$n_2(\mathbf{r},t) = \int f_2(\mathbf{r},\mathbf{p},t)d^3p\,. \tag{17}$$

Then, taking into account the above, the defining system of equations will represent nothing else:

$$\begin{cases} \dfrac{\partial n_2}{\partial t} = A_{21}n_2 - w_{21}n_2 + w_{12}n_1 + \dfrac{1}{4\pi}\int\oint L_\nu(\mathbf{r},\hat{\mathbf{l}})\left[B_{12}n_1 - B_{21}n_2\right]P(\nu)d\hat{\mathbf{l}}d\nu, \\ (\hat{\mathbf{l}},\nabla)L_\nu(\mathbf{r},\hat{\mathbf{l}}) = -\varepsilon_\nu(\mathbf{r}) + \kappa_\nu(\mathbf{r})L_\nu(\mathbf{r},\hat{\mathbf{l}}), \end{cases} \tag{18}$$

where $P(\nu)$ is a function of the contour of the spectral line of radiation, A_{21}, B_{12} & B_{21} are the Einstein coefficients, $e_\nu(\mathbf{r})$ and $k_\nu(\mathbf{r})$ are the emission and absorption coefficients, respectively. Using the equations of state of an ideal gas (Boltzmann's and Saha's laws), we can calculate the composition of the discharge plasma.

It is not difficult to prove that the integral expression of the system of equations (18) is:

$$\frac{1}{4\pi}\int\oint L_\nu(\mathbf{r},\hat{\mathbf{l}})\left[B_{12}n_1 - B_{21}n_2\right]P(\nu)d\hat{\mathbf{l}}d\nu =$$

$$= \frac{B_{12}n_1 - B_{21}n_2}{4\pi}\int\oint L_\nu(\mathbf{r},\hat{\mathbf{l}})\left[B_{12}n_1 - B_{21}n_2\right]P(\nu)d\hat{\mathbf{l}}d\nu = \frac{B_{12}n_1 - B_{21}n_2}{4\pi}\int E_0(\mathbf{r},\nu)P(\nu)d\nu\,,$$

where $E_0(\mathbf{r},\nu)$ - spatial irradiance, which is calculated:

$$E_0(\mathbf{r},\nu) = \oint L_\nu(\mathbf{r},\hat{\mathbf{l}})d\hat{\mathbf{l}} = \oint\int_0^\xi \varepsilon_\nu(\mathbf{r}-t\hat{\mathbf{l}})\exp(-\kappa_\nu t)\frac{t^2}{t^2}dtd\hat{\mathbf{l}} =$$

$$= \int_V \varepsilon_\nu(\mathbf{r}')\frac{\exp(-\kappa_\nu|\mathbf{r}-\mathbf{r}'|)}{|\mathbf{r}-\mathbf{r}'|^2}d^3r' \tag{19}$$

Let's define an auxiliary function – the radiation transfer operator:

$$\mathrm{K}\left(|\mathbf{r}-\mathbf{r}'|\right) = \frac{1}{4\pi}\int\kappa_\nu(\mathbf{r}')P(\nu)\frac{\exp(-\kappa_\nu|\mathbf{r}-\mathbf{r}'|)}{|\mathbf{r}-\mathbf{r}'|^2}d\nu\,. \tag{20}$$

Then, taking into account all substitutions, we obtain the resulting equation characterizing the excitation transfer in a low-temperature gas-discharge plasma:

$$\frac{\partial n_2}{\partial t} = A_{21}n_2 - w_{21}n_2 + w_{12}n_1 + \int_V A_{21}n_2(\mathbf{r}')\mathrm{K}\left(|\mathbf{r}-\mathbf{r}'|\right)d^3r'\,. \tag{21}$$

To effectively solve this problem, it is necessary to use special databases containing information about the emission spectra of various elements and particles [12].

2.1. The software used in the research

There are several types of software tools for modeling and visualization of low-temperature gas-discharge plasma. Table 1 shows their main features.

Table 1 – Comparison of software tools

Software tools	Advantages	Limitations and disadvantages
ANSYS Plasma Simulation	Provides high simulation accuracy, allowing you to analyze a variety of plasma parameters	Requires significant computing power, especially for complex models

CST Studio Suite	Provides tools for visualization and analysis of electromagnetic and plasma phenomena	The initial specialization in electromagnetic modeling limits the analysis of radiation phenomena
PlasmaLab	It is effective for narrowly focused tasks in the field of plasma	It is not universal and may be limited in the possibilities for modeling other physical processes
OpenFOAM	Open source software with flexible capabilities for flow modeling and heat transfer	Requires additional adaptation and configuration for plasma modeling
COMSOL Multiphysics	It has multitasking and flexibility: it allows you to integrate various physical phenomena into a single model, provides a wide selection of various physical models	It will take some time to master due to the richness of functionality and complexity

Based on the conducted analysis (Table 1), it is recommended to give preference to COMSOL Multiphysics [13].

It is important to note that this software suite utilizes the Finite Element Method (FEM) to solve the system of equations (1-13). This method is based on decomposing complex domains or systems into simpler subdomains with unique geometric and mathematical characteristics. In other words, the problem is divided into a finite number of sub-problems, which are then solved using numerical methods. This approach allows for obtaining more detailed and accurate results for complex systems, considering various physical interactions. The main interface of the program provides a graphical environment where the user can create the model's geometry, specify boundary conditions, material properties, and other parameters.

Let's outline the main steps that can be taken when modeling in COMSOL:

1. Geometry Creation: COMSOL tools allow the creation of complex three-dimensional geometries using an intuitive user interface or importing models from other CAD programs.
2. Definition of Material Properties: Define the physical properties of the materials used in the model.
3. Introduction of Boundary Conditions: Specify boundary conditions for various surfaces in the model.
4. Setting up the Core System of Equations.
5. Solving the Model: As mentioned earlier, the COMSOL Plasma Module uses numerical methods to solve the system of equations describing the physical processes in the model.
6. Results Analysis: After completing the calculation, it is necessary to analyze the modeling results. Various program modes are used for this purpose:

- The "Cross-Section Plot Parameters" mode allowed to explore the parameters of the model by creating cross-sections of a three-dimensional object.
- The "Domain Plot Parameters" mode was used to study variables at the boundary of the object partition area. The "Arrow Plot" mode is for visualization of a vector microwave field.
- "Slice" mode - to display the task parameters in the selected plane using a color scale.

These steps represent an optimal modeling process that can be easily adapted depending on the introduction of additional boundary conditions or parameters.

The implementation of spatial modeling of a coaxial cylindrical tube simulating a mercury-argon discharge is shown in Figure 1, following the above-described algorithm.

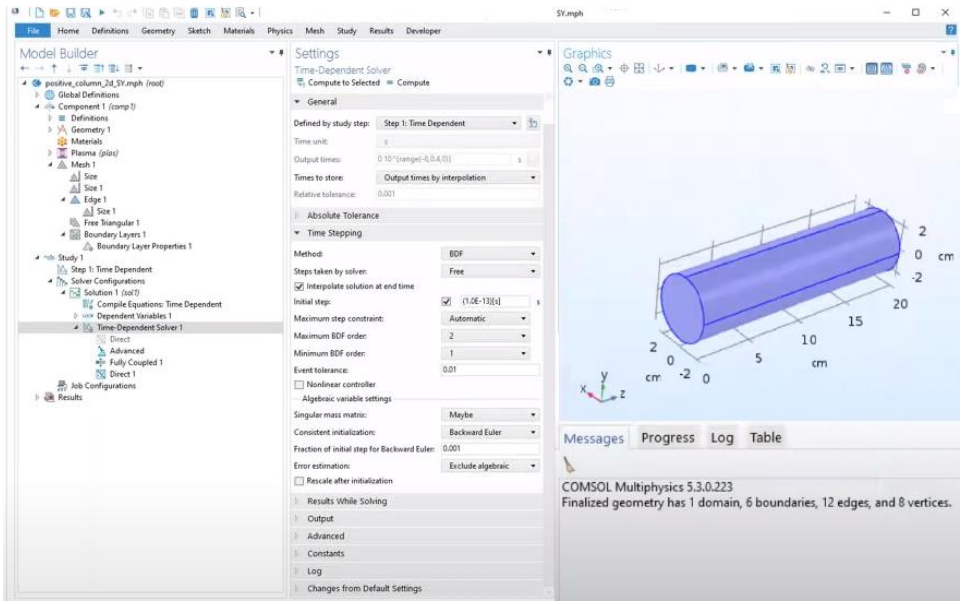

Fig. 1. An example of modeling a cylindrical radiator in COMSOL Multiphysics

COMSOL Multiphysics provides the capability to visualize the mesh in a graphical window, allowing users to add, delete, change the sizes and shapes of nodes and elements, and adjust the mesh density in necessary areas. This allows for incrementally increasing the number of mesh points in regions where the electric field intensity changes the most. Using successive iterations to improve mesh accuracy in areas with high electric field intensity changes is an effective strategy to achieve more accurate results and meet accuracy criteria in these regions.

For the calculations, a cluster node with 10 CPU cores and 32 GB of RAM was deployed. Since the CPU cores are consistently loaded at approximately 100% throughout the entire calculation time, and memory usage remains low (not exceeding 30%), it indicates that the CPU handles the majority of the computations. In this configuration, the use of graphics accelerators (GPUs) is not required and does not significantly impact the performance of calculations and visualization.

However, if there is a future need for tasks that can be efficiently parallelized using GPUs, considering adding GPUs to the current configuration is worth considering. GPUs can be beneficial for certain types of computational tasks, such as deep learning neural networks or scientific calculations, where numerous parallel computations can be efficiently performed using CUDA and similar graphical libraries.

3. Simulation results and their discussion

As a result of the calculations, 3D visualization data of numerical simulation of a microwave discharge in a mercury-argon low-temperature plasma were obtained.

Figures 2 and 3 show the radial and spatial distributions of the concentrations of excited mercury atoms. The radial distribution of resonant atoms displays their concentration depending on the radius and vertical coordinate of the plane. The spatial distribution of concentration shows the distribution of concentration throughout the entire volume of the model.

Both distributions were obtained using the Slice mode in the COMSOL Multiphysics program, which allowed visualizing selected slices or planes inside the model for more detailed data analysis.

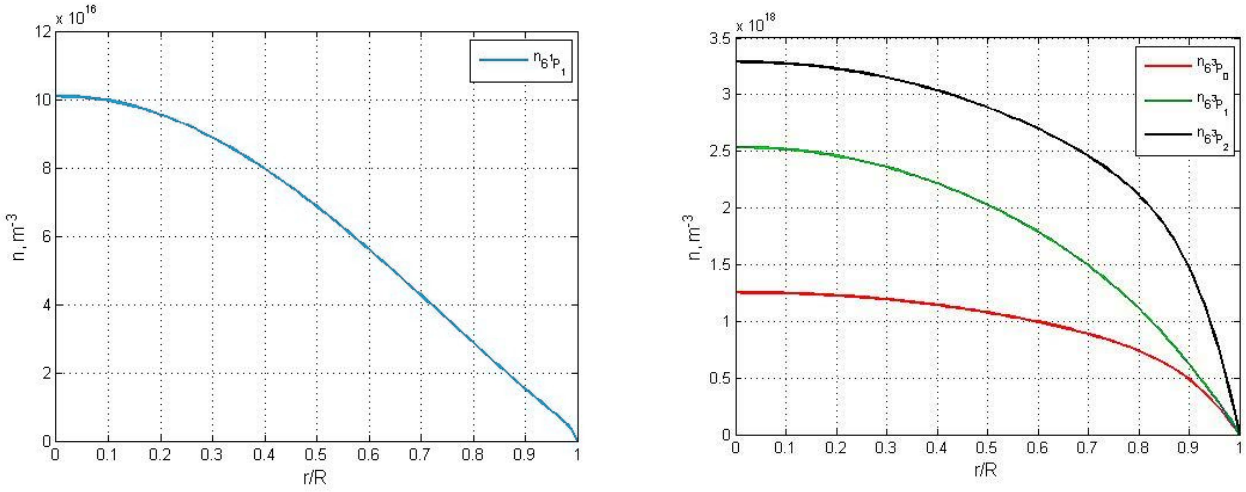

Fig. 2. Radial distributions of concentrations of excited mercury atoms.

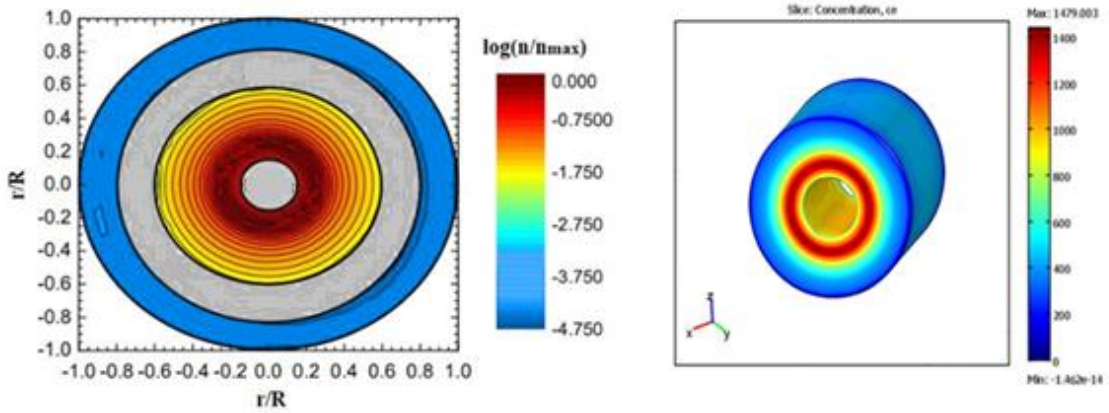

Fig. 3. Spatial distribution of concentration in the central plane $z = L/2$

In Figure 2, one can observe the processes associated with photons falling into the area behind the reflecting obstacle as a result of reabsorption processes. The use of local cross sections inside the object under study made it possible to reveal its internal structure and features of parameters in three-dimensional visualization. The local sections here were planes that intersect the object at certain points, which contributed to a more detailed study of the internal components of the object. The result of visualization of the electron concentration in the discharge is shown in Figure 3, where $c_e = n_e/n_c$. Here n_e – electron concentration, $n_c = 7 \cdot 10^{10}$ cm^{-3} - peak concentration.

To more vividly illustrate the influence of the non-uniformity of absorbing atoms (in this case, neutrals) on the distribution of emitting (in this case, resonant) particles, let's analyze the Green's functions. These functions allow us to find the solution to the transport equation in the form:

$$n(\mathbf{r}) = \int_V G(\mathbf{r}, \mathbf{r}') W(\mathbf{r}') d^3 r' . \qquad (22)$$

The dependences for homogeneous and inhomogeneous plasma obtained using MATLAB are shown in Figure 4.

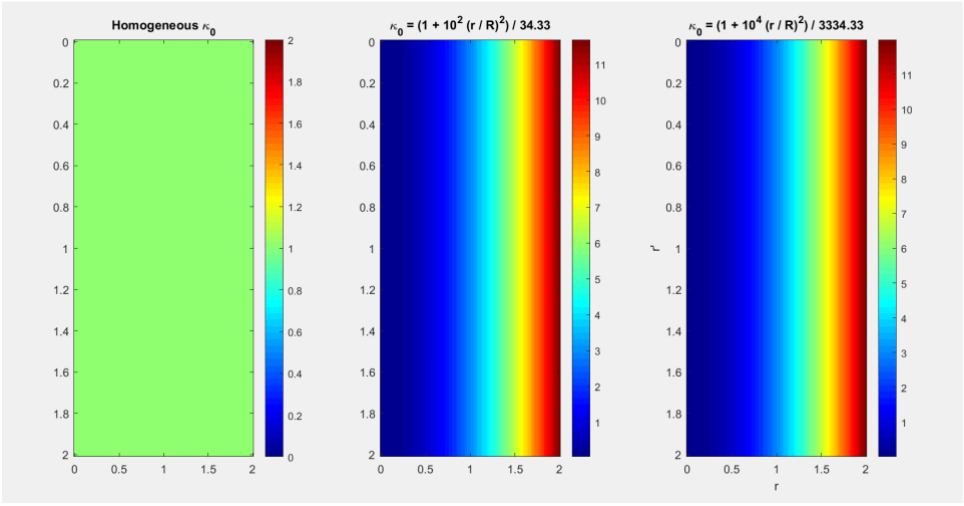

Fig. 4. Green's functions of the radiation transfer operator for homogeneous (1) and inhomogeneous absorption at $\kappa_0(r) = 10^2\,(r/R)^2\,/33.34$ (2) & $\kappa_0(r) = 10^4\,(r/R)^2\,/3334.33$ (3).

In particular, it is easy to prove that in an optically homogeneous plasma, in which the contour function of the spectral line $P(\nu)$ does not depend on the coordinate, the symmetry condition $G(\mathbf{r},\mathbf{r}') = G(\mathbf{r}',\mathbf{r})$ is satisfied.

These functions allow for a more detailed exploration of the spectral characteristics of radiation and its spatial distribution.

Now, let's assess the change in gas temperature along the discharge cross-section. To do this, we will consider the heat conduction equation in a steady-state, taking into account that elastic collisions with argon and mercury atoms have a significant impact on the heating process of gas atoms and the establishment of the radial temperature profile T:

$$-\frac{1}{r}\frac{d}{dr}rK_T(T)\frac{d}{dr}T = W_{ec,Hg} + W_{ec,Ar}\,, \tag{23}$$

where $K_T(T)$ – coefficient of thermal conductivity of a mixture of gases, $W_{ec,Hg} + W_{ec,Ar}$ – the power transmitted to argon and mercury atoms by electrons per unit volume of plasma. The boundary conditions for (23) are written as follows:

$$\left.\frac{d}{dr}T\right|_{r=0} = 0,\;\; T(R) = T_{wall}\,, \tag{24}$$

and $W_{ec,Hg}$ & $W_{ec,Ar}$:

$$W_{ec,Hg} = n_e(r)\frac{p_{Hg}}{kT}\frac{2m_e}{M_{gas}}\int_0^\infty \frac{m_e v^2}{2} v q_{Hg}(v) f_e(v) dv\,, \tag{25}$$

$$W_{ec,Ar} = n_e(r)\frac{p_{Ar}}{kT}\frac{2m_e}{M_{gas}}\int_0^\infty \frac{m_e v^2}{2} v q_{Ar}(v) f_e(v) dv\,. \tag{26}$$

Since the process of forming the radial distribution of gas temperature is caused by elastic collisions of electrons with mercury and argon atoms, the Maxwell function can be taken as the electron velocity distribution function (EVDF) $f_e(v)$:

$$f_e(v) = 4\sqrt{\frac{m_e}{2\pi k T_e}}\frac{m_e v^2}{2kT_e}\exp\left[-\frac{m_e v^2}{2kT_e}\right]. \tag{27}$$

As $n_e(r)$ it is convenient here to take the Bessel distribution with zero on the wall of the bulb: $n_e(r) = n_{e0} J_0(2.405 r / R)$.

Figure 5 shows the calculated gas temperature distributions for three pressures (0.1, 0.5 and 1 Torr).

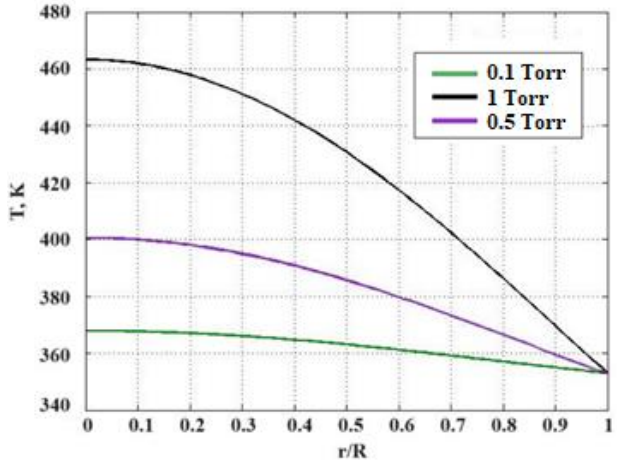

Fig. 5. Radial temperature distributions in a mercury-argon discharge

To determine the distribution of the electric field in a discharge, various experimental methods are commonly used in practice, such as microwave spectroscopy [14] or the use of electrostatic probes [15]. However, these methods require expensive equipment and high-precision measuring instruments. This problem has been addressed by combining the use of the Comsol Multiphysics software and a specialized algorithm developed in Matlab.

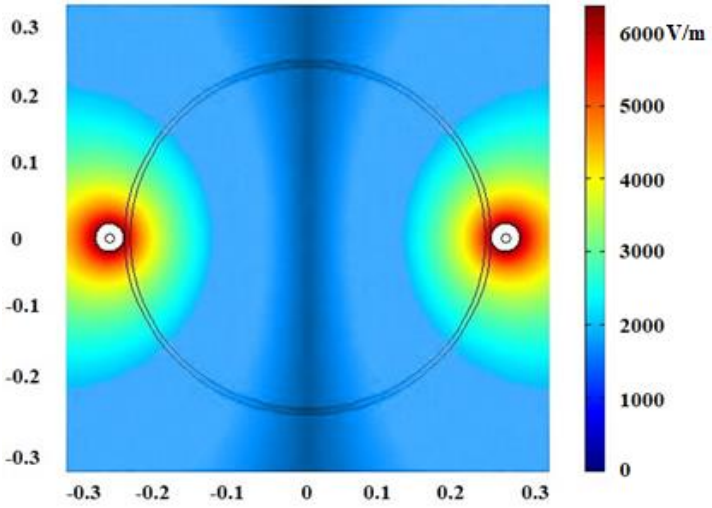

Fig. 6. Spatial distribution of the electric field intensity modulus.

From Figure 6, it can be seen that the electric field intensity reaches its maximum at the tube walls and then rapidly decreases as it propagates through the plasma cross-section. At the same time, the maximum volume power density is observed slightly closer to the center of the tube due to the low electron concentration at the walls. When changing the collision frequency in the plasma due to variations in dielectric permittivity, only minor changes are observed in the distribution of the electric field. The electric field periodically oscillates along the axial direction, but in the radial direction, it remains close to a uniform distribution. This is important for analyzing the behavior of the parameter S11 at different plasma frequencies. S11 represents the reflection coefficient of the microwave wave from the device input and is determined as the ratio of the complex amplitude of the reflected wave to the complex amplitude of the incident wave (see Figure 7).

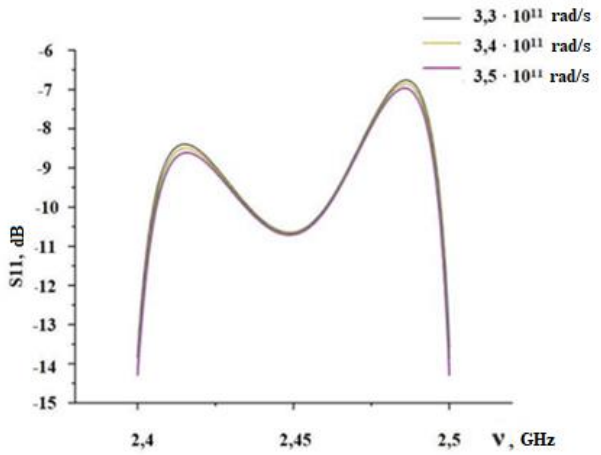

Fig. 7. Distribution of S11 at different plasma frequencies

If the reflection coefficient (S11) is below -10 dB, as shown in Figure 7, it indicates a low level of reflected power, which is a measure of efficiency. When the reflected power remains consistently low and hardly changes with varying plasma frequencies, it suggests that the considered structure is adapted to work with different radiation sources. Thus, maintaining a low value of S11 regardless of the plasma frequency is an important condition for the effective operation of this device.

Figure 8 presents the dependence of the reflection coefficient S11 on the parameter W_h, which represents the width of all resonator slits, at a frequency of 2.45 GHz. At different values of slit width, the microwave system reaches resonance at the operating frequency, and accordingly, S11 increases with increasing values of W_h. When W_h is equal to 17 mm, S11 exceeds -10 dB, indicating that acceptable S11 values are achieved only with slit widths ranging from 9 to 16 mm. These slits facilitate the coupling of microwave energy as they restrict the discharge current and transfer microwave energy from the source along all the slits. The geometric arrangement of the slits also affects the amount of output optical radiation energy. Based on the above, the optimal value of the parameter W_h was chosen to be 16 mm. In this case, S11 is -10.13 dB, and the absorption efficiency reaches 92%.

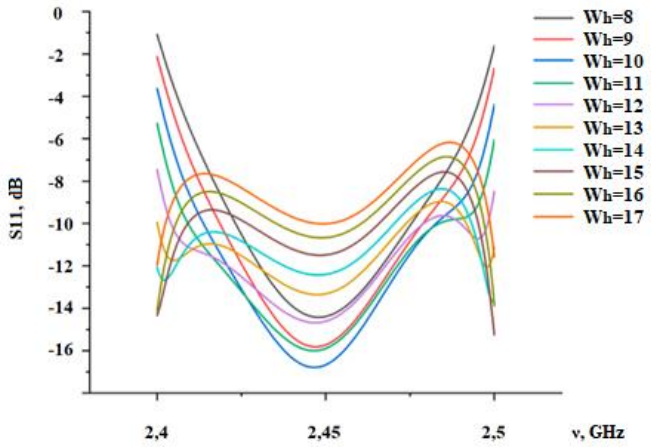

Fig. 8. Comparison of S11 values when changing parameter W_h.

As a result, visualization of the obtained simulation data allowed adjustments in the design of the optical radiation source considered in the work, which led to an increase in the efficiency of the system by 8% compared to [16]. The drawing of the developed radiator model is shown in Figure 9.

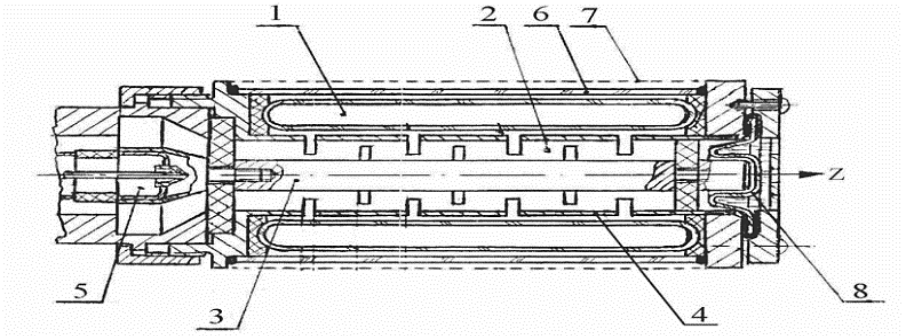

Fig. 9. Drawing of an electrodeless microwave optical radiation source. 1 – cylindrical optical radiation source; 2 – coaxial path; 3 – central conductor of the path; 4 – outer conductor of the path with transverse microwave emitting slots; 5 - magnetron output device; 6 – microwave transparent cover; 7 – removable microwave screen; 8 – plug.

According to Figure 9, the cylindrical resonator consists of a quartz tube with a length of 200 mm, an inner diameter of 8 mm, and an outer diameter of 12 mm. Inside the tube, there is argon at a pressure of p_{Ar} = 0.75 Torr and mercury at $p_{Hg} \approx$ 0.05 Torr. The resonator includes a quartz tube that passes through its axis of symmetry. It's worth noting that the external part of this tube, extending beyond the resonator, has the same length. Around the upper and lower metal plates of the resonator, there is a cylinder of larger diameter that encircles the quartz tube.

The TEM wave source is represented by a magnetron operating at a frequency of 2.45 GHz and is positioned on top of the waveguide in such a way that its lower cross-section is located on the upper plate of the cylindrical resonator. Additionally, the central coaxial electrode is introduced into the resonant cavity, with its end positioned in the middle between the upper and lower plates of the resonator. The quartz tuning rod is in a horizontal plane and is introduced into the resonator through the lateral wall.

Thus, the main parameters of the developed source are presented in Table 2.

Table 2 – Source parameters used in modeling

Parameter	Physical meaning	Value
W_h	Width of all slots	16 mm
Φ	The central angle of all metal grooves	315◦
D	Outer diameter of the inner conductor of the coaxial radiator	8 mm
d	Inner diameter of the outer conductor of the coaxial radiator	12 mm
L	Total length of the coaxial radiator	200 mm
1_1	The distance from the center of the first slot to the short circuit surface	15 mm
l_2	The distance between adjacent metal centers with slots	18 mm
p_{Ar}	Argon operating pressure	0,75 Torr
p_{Hg}	Mercury operating pressure	0,05 Torr
P_{input}	Input power	687 W
ν	Microwave frequency	2,45 GHz

A photo of the source in working condition is shown in Figure 10.

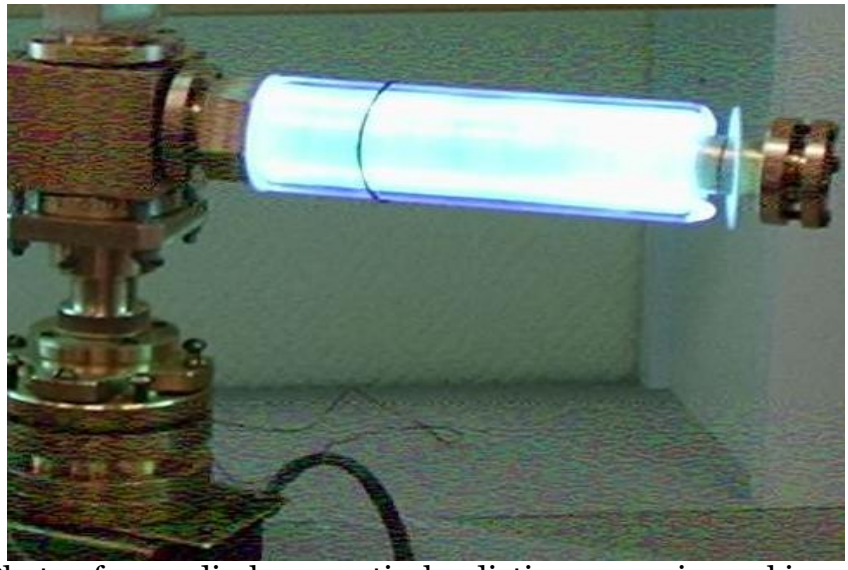

Fig.10. Photo of a gas-discharge optical radiation source in working condition

4. Conclusions

Therefore, the development of software-hardware complexes aimed at data visualization and improving information representation in the context of modeling low-temperature gas discharge plasma and related physical processes remains a highly important and relevant aspect in this research field. Software solutions and specialized tools designed for this direction play a crucial role in aiding the understanding and improvement of various aspects of gas discharge phenomena.

Addressing the issues of creating specialized distributed environments for simulating gas discharge opens up prospects for more accurate and reliable numerical calculations. This, in turn, can have practical applications in the development of new technologies, such as gas discharge optical radiation sources.

The use of computer graphics for data visualization allows researchers to delve more deeply into the modeling and analysis of results. It enables the identification of not only general patterns but also details of the internal structure and parameter distribution within the discharge medium.

The visualization results of the mercury-argon plasma model in the coaxial microwave discharge presented in this work make a significant contribution to the understanding of this physical phenomenon. Local sections of the computational domain allowed for a more detailed investigation of the internal aspects of the plasma, which can be valuable in the development of new devices and optical radiation sources. Based on the modeling conducted in this work, the design of a coaxial gas discharge optical radiation source has been developed.

References

1. Gadzhiev M.H., Emirov R.M., Muslimov A.E., Ismailov M.G., Kanevsky V.M. Formation of superhard coatings during treatment of titanium films with low-temperature nitrogen plasma in an open atmosphere / Letters to the Journal of Technical Physics. – 2021. – Vol. 47, No. 9. – pp. 44-47.

2. Ermolaeva S.A., Petrov O.F., Miller G.G., Shaginyan I.A., Naroditsky B.S., Sysolyatina E.V., Mukhachev A.Ya., Morfill G.E., Fortov V.E., Grigoriev A.I., Ginzburg A.L. Prospects the use of low-temperature gas plasma as an antimicrobial agent / Bulletin of the Russian Academy of Medical Sciences. – 2011. – No. 10. – pp. 15-21.

3. Lazukin A.V., Ermakov A.M., Afanasyeva V.A. Development of a low-temperature gas plasma generator for medical use and the prospect of its use as an effective sterilizer and activator of wound healing in field and stationary conditions in the medical service of the Russian Army / Izvestiya Institute of Engineering Physics. – 2021. – № 3(61). – Pp. 91-93.
4. Maslennikov O.P., Milman I.E., Safiullin A.E. , Bondarev A.E., Nizametdinov Sh.U., Pilyugin V.V. Development of a system of interactive visual analysis of multidimensional data / Scientific visualization. 2014. No. 4. pp. 30-49.
5. Bondarev A.E., Galaktionov V.A. Analysis of multidimensional data in multiparametric optimization problems using visualization methods / Scientific Visualization. Vol.4, No. 2, pp.1-13, 2012
6. Zheleznov I.I., Popov O.A. Investigation of the radiative and spectral characteristics of UV radiation sources based on coaxial microwave discharges in low-pressure mercury vapor // Vestnik of the MPEI. 2023. No. 2. pp. 137-143.
7. Kalyazin Yu.F., Kokinov A.M., Malkov M.A.. Mathematical model for calculating the characteristics of a low-pressure mercury-gas discharge // "Lighting Engineering", 2003, No. 2, pp. 2-5.
8. Radzig A.A., Smirnov B.M. Parameters of atoms and atomic ions, handbook // Moscow: Energoatomizdat, 1986.
9. Rokhlin G.N. Discharge light sources // M. Energoatomizdat. 1991. 720c.
10. R. Reed, J. Prausnitz, T. Sherwood. Properties of gases and liquids // L.: Khimiya, 1982, 592s.
11. Maimistov A.I., Lyashko E.I. Modified Drude-Lorentz model, allowing to take into account the topological characteristics of the medium // Optics and spectroscopy. 2019. Vol. 127. No. 11. pp. 804-810.
12. Lebedev Yu.A., Yusupova E.V. The effect of a constant field on the near-surface plasma of a highly inhomogeneous microwave discharge. Plasma physics. 2012. Vol. 38. No. 8. pp. 677-693.
13. COMSOL 3.5a http://www.comsol.com
14. Moustafaev, J. Project Scope Management: A Practical Guide to Requirements for Engineering, Product, Construction, IT and Enterprise Projects (1st ed.). Auerbach Publications. (2014). https://doi.org/10.1201/b17797
15. Demidov V.I., Kolokolov N.B., Kudryavtsev A.A. Probe methods of low-temperature plasma research. M. Energoatomizdat. 1996.
16. Zheleznov I. I., Popov O. A. Electrodeless source of UV radiation based on low pressure microwave mercury discharge // Light & Engineering. 2023. Vol. 31, No. 3. P. 36-42.